Carbon-related matrix effects in inductively coupled plasma atomic emission spectrometry

ARTICLE *in* SPECTROCHIMICA ACTA PART B ATOMIC SPECTROSCOPY · FEBRUARY 2008

Impact Factor: 3.18 · DOI: 10.1016/j.sab.2007.11.024

4 AUTHORS, INCLUDING:

Guillermo Grindlay
University of Alicante
22 PUBLICATIONS **187** CITATIONS
SEE PROFILE

Luis Gras
University of Alicante
45 PUBLICATIONS **432** CITATIONS
SEE PROFILE

Juan Mora
University of Alicante
50 PUBLICATIONS **815** CITATIONS
SEE PROFILE

ELSEVIER

Spectrochimica Acta Part B 63 (2008) 234–243

SPECTROCHIMICA ACTA PART B

www.elsevier.com/locate/sab

Carbon-related matrix effects in inductively coupled plasma atomic emission spectrometry ☆

G. Grindlay [a,*], L. Gras [b], J. Mora [b], M.T.C. de Loos-Vollebregt [a]

[a] *Faculty of Applied Sciences, DelftChemTech, Julianalaan 136, 2628 BL Delft, The Netherlands*
[b] *Department of Analytical Chemistry, Nutrition and Food Sciences, University of Alicante, P.O. Box 99, 03080, Alicante, Spain*

Received 5 November 2007; accepted 16 November 2007
Available online 23 November 2007

Abstract

In Inductively Coupled Plasma Atomic Emission Spectrometry (ICP-AES), it has been observed that the emission intensity of some atomic lines is enhanced or depressed by the presence of carbon in the matrix. The goal of this work was to investigate the origin and magnitude of the carbon-related matrix effects in ICP-AES. To this end, the influence of the carbon concentration and source (i.e. glycerol, citric acid and potassium hydrogen phthalate), the experimental conditions and sample introduction system on the aerosol characteristics and transport, plasma excitation conditions and the emission intensity of several atomic and ionic lines of a total of 15 elements has been studied. Results indicate that carbon related matrix effects do not depend on the carbon source and they become more severe when the amount of carbon loaded into the plasma increases, i.e., when using: (i) carbon concentrations higher than 5 g L^{-1}; (ii) high sample uptake rates; and (iii) efficient sample introduction systems. Thus, when introducing carbon into the plasma, the emission intensity of atomic lines with excitation energies below 6 eV is depressed (up to 15%) whereas the emission intensity of atomic lines of higher excitation energies (i.e. As and Se) are enhanced (up to 30%). The emission intensity of the ionic lines is not affected by the presence of carbon. The origin of the carbon-related interferences on the emission intensity of atomic lines is related to changes in the line excitation mechanism since the carbon containing solutions show the same aerosol characteristics and transport efficiencies as the corresponding aqueous solutions. Based on the previous findings, a calibration approach for the accurate determination of Se in a Se-enriched yeast certified material (SELM-1) has been proposed.

Keywords: Carbon; Organic; Matrix effects; Inductively coupled plasma; Atomic emission spectrometry

1. Introduction

Carbon is a concomitant element in biological, environmental and petrochemical samples. Most of the studies in plasma techniques (Inductively Coupled Plasma Atomic Emission Spectrometry, ICP-AES, and Inductively Coupled Plasma Mass Spectrometry, ICP-MS) related to this element have been focused on the influence of organic solvents on the aerosol generation and transport, as well as, on the plasma characteristics [1–3]. Results reported in the literature indicate that organic solvents effects depend on both solvent nature and sample introduction system [3,4]. Due to their physical properties, organic solvents use to generate finer pneumatic aerosols and give rise to higher aerosol transport than pure aqueous solutions [5]. As a consequence an improvement in the analyte signal is expected. Nonetheless, also the solvent load into the plasma is increased and the plasma excitation conditions may be deteriorated and, therefore, a reduction in the expected signal can also be observed [6]. The deleterious effect of organic solvents on the plasma excitation/ionization capabilities can be minimized by appropriate selection of the

☆ This article is published in a special honor issue dedicated to Jim Winefordner on the occasion of his retirement, in recognition of his outstanding accomplishments in analytical atomic and molecular spectroscopy.

* Corresponding author. Work performed while on leave from the Department of Analytical Chemistry, Nutrition and Food Sciences, University of Alicante, Alicante, Spain.
E-mail address: guillermo.grindlay@ua.es (G. Grindlay).

0584-8547/$ - see front matter © 2007 Elsevier B.V. All rights reserved.
doi:10.1016/j.sab.2007.11.024

experimental conditions and sample introduction characteristics [7–14]. Hu et al. [15] observed that in ICP-MS, the enhancement or suppression of the analyte signals due to the presence of organic solvents depends, in addition to the solvent nature, sample introduction system and operating conditions, on: (i) the ion mass. For a given organic solvent concentration, the enhancement effect was less significant when increasing the analyte ion mass due to the spatial shift of the zone of maximum ion density; and (ii) the ionization potential (IP) of the element concerned. Signal enhancements of elements with IP between 9 and 11 eV (e.g. Be, Se, As, Au, I, P, S,…) were higher than those of elements with about the same mass/charge ratio and low IPs values. Similar results have been reported by other authors [16–19]. Thus, Allain et al. [16] reported a signal enhancement for Hg (600%), As (240%), Au (325%) and Se (250%) when a 36 g L^{-1} carbon (as glycerol) solution was introduced into the ICP-MS. To explain these findings, some authors suggested a charge transfer mechanism between the analyte atoms and carbon positively charged ions [20,21]. The charge transfer reaction is only possible when the analyte has a similar IP as carbon, so that elements with low IP (i.e. Na, Ca, Mg,…) are not influenced by this interference. The magnitude of the signal enhancement is related to the amount of carbon in the plasma. For higher carbon concentrations, interferences are more pronounced [16,22]. Similar behavior was obtained using other carbon sources such as acetic acid [23], acetone [15,24], alcohols [18,22], ethylendiamine [25], ammonium carbonate [26] or methane [27].

In ICP-AES, the effect of the presence of carbon containing compounds in the matrix has not been investigated in detail. Long et al. observed that introduction of propane into the plasma changes the emission intensity of some atomic lines [28]. Thus, when introducing 20 mL min^{-1} of propane, the signal for the Al I 396.2 nm emission line was enhanced by 20%. However, for the Ca I 422.7 nm line, a 50% signal reduction was obtained. These results were attributed to chemical reactions and changes in line excitation mechanisms. Machat et al. [29,30] focused a study on several Se atomic lines and observed that the emission intensity was enhanced due to the presence of carbon in the matrix. Thus, when nebulizing glycerol solutions containing up to 20 g L^{-1} of carbon, the emission intensity was enhanced by 20% and 60% for Se at 196.026 nm and 199.511 nm, respectively [30]. Similar behaviour was obtained when Se was introduced into the ICP as hydride together CO_2. These authors suggested a complex line excitation mechanism between Se and carbon species [30] that would explain simultaneously the Se signal enhancements observed in both ICP-MS and ICP-AES.

The aim of this work was to evaluate carbon-related matrix effects on the analytical response of several atomic and ionic emission lines of a total of 15 elements in ICP-AES. To this end, the influence of the carbon source (i.e. glycerol, citric acid and potassium hydrogen phthalate) and concentration, experimental conditions (i.e. sample uptake rate, nebulizer gas flow and r.f. power) and the sample introduction system on the aerosol generation and transport, the plasma characteristics and the emission intensity were studied. Finally, the results of this study were applied to the analysis of a certified Se-enriched yeast sample (SELM-1).

2. Experimental

2.1. Reagents and samples

Test solutions containing 20 mg L^{-1} of Se and As, plus 5 mg L^{-1} of different analytes were prepared by diluting aliquots from 1000 mg L^{-1} Se and As mono-elemental (Merck, Darmstadt, Germany) and multi-elemental ICP reference solution (ICP-IV, Merck, Darmstadt, Germany) in deionized water and as carbon containing solutions containing glycerol, citric acid or potassium hydrogen phthalate (Sigma-Aldrich, Steinheim, Germany).

Solutions used to measure the analyte transport rate were prepared from $MnCl_2{\cdot}4H_2O$ and $CuSO_4$ (Panreac, Castellar del Valles, Spain).

A certified Se-enriched yeast (SELM-1, National Research Council, Ottawa, Ontario, Canada) was analyzed after a digestion treatment in a microwave oven (MSP 1000, CEM, Matthews, North Carolina, USA) using the program recommended by the manufacturer for this type of samples. Analytical grade nitric and hydrochloric acids (Sigma-Aldrich, Steinheim, Germany) were employed for the digestion procedure.

2.2. ICP instrumentation

ICP-AES measurements were mainly performed using a PerkinElmer Optima 3000 DV ICP-AES (PerkinElmer, Shelton, CT, USA). A PerkinElmer Optima 4300 DV ICP-AES was used in Alicante to study the influence of the sample introduction system on carbon-related matrix effects. Samples were introduced in the Optima 3000 DV via a cross-flow nebulizer coupled to a Ryton double-pass spray chamber whereas for the Optima 4300 DV the sample introduction system consisted of a high efficiency nebulizer (HEN, Meinhard Glass Products, Santa Ana, CA, USA) coupled to a standard cyclonic spray chamber or a low-volume cyclonic spray chamber (Cinnabar, Glass Expansion, Australia). Operating conditions used with both instruments are shown in Table 1.

A total of 32 analytical lines of 15 elements covering a wide range of E_{sum} values, defined as the sum of excitation energy (E_{exc}) and ionization energy (E_{ion}) (Table 2), were studied. All measurements were performed in axial viewing mode since, with the experimental arrangement used, the sensitivities for the As and Se lines were too low in the radial viewing mode.

Table 1
Operating ICP-AES conditions with the different instruments employed

	Optima 3000 DV	Optima 4300 DV
Plasma forward power/W	950–1450	1450
Argon flow rate/L min^{-1}		
Plasma	15	15
Auxiliary	0.5	0.2
Nebulizer (Q_g)	0.5–0.7	0.6
Sample uptake rate (Q_l)/mL min^{-1}	0.3–1.5	0.1–0.4
Sample introduction		
Nebulizer	Cross-flow	HEN
Spray chamber	Double pass	Standard cyclonic and Cinnabar
Integration time/ms	25	25
Readings/replicates	10/10	10/10

Table 2
Elements, wavelengths and energy values for the selected lines

	Element	Wavelength (nm)	E_{exc} (eV)	E_{ion} (eV)	E_{sum} (eV)
	Sr	460.733	2.69	–	2.69
	Ca	422.673	2.93	–	2.93
	Al	396.153	3.14	–	3.14
	Cr	357.869	3.46	–	3.46
	Ag	338.289	3.66	–	3.66
	Cu	324.752	3.82	–	3.82
Atomic lines	Li	610.632	3.88	–	3.88
	Ar	420.069	3.95	–	3.95
	Mg	285.213	4.35	–	4.35
	Ni	232.003	5.34	–	5.34
	Cd	228.802	5.42	–	5.42
	Pb	217.000	5.70	–	5.70
	Zn	213.857	5.80	–	5.80
	C	193.030	6.22	–	6.22
	Se	203.985	6.32	–	6.08
	As	197.197	6.29	–	6.28
Se and As	Se	196.026	6.32	–	6.32
atomic lines	As	193.696	6.40	–	6.40
	As	188.979	6.56	–	6.56
	Ba	413.065	5.72	5.21	10.93
	Ba	230.425	5.98	5.22	11.20
	Mg	280.271	4.43	7.64	12.07
	Mn	257.610	4.86	7.43	12.29
	Cr	267.716	6.16	6.76	12.92
	Fe	238.204	5.20	7.87	13.07
	Ca	315.887	7.05	6.11	13.16
Ionic lines	Co	228.616	5.84	7.86	13.70
	Ni	221.648	6.63	7.64	14.27
	Cd	214.440	5.78	8.99	14.77
	Pb	220.353	7.37	7.42	14.79
	Zn	206.200	6.01	9.39	15.40
	Cu	224.700	8.23	7.73	15.96
	Mg	279.077	8.86	7.65	16.51
	Ag	243.778	9.94	7.58	17.52

2.3. Aerosol drop size distributions measurements

Aerosol drop size distributions (DSD) were measured by means of a laser Fraunhofer diffraction system (Model 2600c, Malvern Instruments Ltd., Malvern, Worcestershire, UK). All measurements were made at a distance of 1 mm from the nebulizer tip (i.e. primary aerosol) or the spray chamber exit (i.e. tertiary aerosol). A lens with a focal length of 63 mm, which enables the system to measure droplets with diameters between 1.2 and 118 μm, was used. The software employed was the version B.0D. Calculations to transform the energy distribution into aerosol size distribution were made using a model-independent algorithm that does not preclude any particular distribution function. A set of five replicates was performed in each case and the precision of the measurements was always better than 4% RSD.

2.4. Solvent and analyte transport measurements

Solvent and analyte transport measurements were performed by means of direct methods [31]. Solvent transport rate (S_{tot}) was measured by the adsorption of the aerosol in a U-tube filled with silica gel during a 10 min period. By weighing the U-tube before and after the aerosol exposure, the S_{tot} values can be obtained. Analyte transport rate (W_{tot}) measurements were performed by nebulizing a solution containing 200 mg L^{-1} of Mn and Cu during a given period of time (i.e. 15 min) and trapping the aerosol at the exit of the spray chamber with a glass fibre filter (type A/E, 47 mm diameter, 0.3 μm pore size, Gelman Sciences, Ann Arbor, MI, USA). The filter was then washed out into a volumetric flask with 1.0% (w/w) nitric acid. The manganese and copper content in each flask was measured by flame atomic absorption spectrometry. A set of three replicates was performed in each case. The precision of these measurements was always better than 4%.

3. Results

3.1. Carbon-related effects on the emission signal

Fig. 1 shows the relative emission intensity values, I_{rel}, for different emission lines versus the corresponding E_{sum} values using 20 g L^{-1} carbon containing solutions prepared from glycerol and citric acid. I_{rel} is defined as the net emission intensity of the analyte obtained with a carbon containing solution relative to that obtained with an aqueous solution of the same composition but without carbon. Before analyzing the results shown in Fig. 1, it is important to point out that the precision of the emission signal for the different lines tested was, on average, 2% RSD (10 replicates). Therefore, it can be considered that I_{rel} values with error bars below 0.96 and higher than 1.04 range (i.e. exceeding a range of 4% error) indicate matrix effects (dotted lines in Fig. 1). I_{rel} values higher than 1.04 indicate a positive matrix effect (i.e. signal enhancement) whereas values lower than 0.96 indicate a negative matrix effect (i.e. signal suppression).

Results in Fig. 1 indicate that the presence of carbon in the matrix strongly affects the emission intensity of some of the lines. The magnitude of the carbon-related matrix effects (I_{rel}) depends on the energy sum and type of the line considered. For atomic lines, different behaviour was observed. On one hand, the intensity for atomic lines with E_{sum} values below 6 eV was

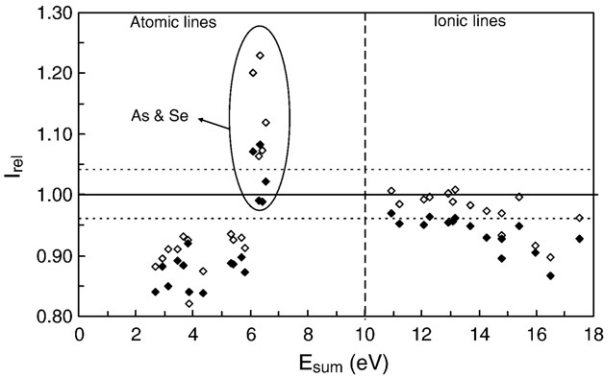

Fig. 1. Relative emission intensity (I_{rel}) obtained with a carbon containing solution in comparison to the corresponding solution without carbon for lines of different E_{sum} values. Carbon sources: (♦) glycerol; (◇) citric acid. I_{rel} values among dotted lines indicate no matrix effects. Carbon concentration 20 g L^{-1}. R.f. power 1450 W; Q_g 0.7 L min^{-1}; Q_l 1.0 mL min^{-1}.

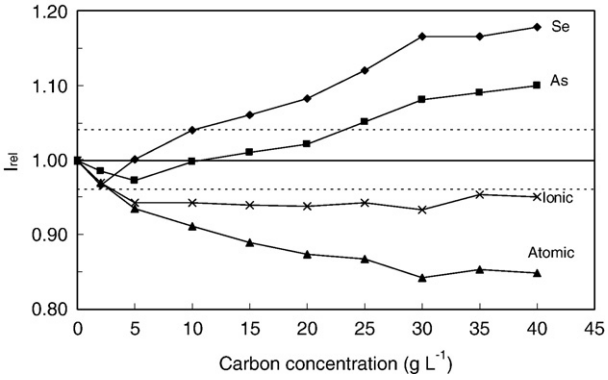

Fig. 2. Influence of the carbon concentration on the I_{rel} values for different type of lines using glycerol as the carbon source: (♦) Se I (196.026 nm); (■) As I (188.979 nm); (▲) atomic lines E_{sum}<6 eV; (×) ionic lines. I_{rel} values among dotted lines indicate no matrix effects. Solution pH: 1.8. R.f. power 1450 W; Q_g 0.7 L min^{-1}; Q_l 1.0 mL min^{-1}.

depressed, on average, by 10% for glycerol and 13% for citric acid solutions, whereas the intensity of atomic lines with E_{sum} values above 6 eV was enhanced. These lines correspond to Se and As (Table 2). The highest signal improvements were obtained at the wavelengths of 196.026 nm (for Se) and 188.979 nm (for As). When the citric acid solution was nebulized, I_{rel} at these Se and As lines was 1.23±0.03 and 1.12±0.02, respectively. Finally, results in Fig. 1 indicate that the intensity of ionic lines with E_{sum}>10 eV is not significantly influenced by the presence of carbon in the matrix. Only for ionic lines with E_{sum} values above 14 eV some decrease in I_{rel} was observed. Fig. 2 shows the influence of the carbon concentration (as glycerol) on the I_{rel} values obtained for Se 196.026 nm and As 188.979 nm. In addition, the averaged I_{rel} values for the atomic lines with E_{sum} below 6 eV and for the ionic lines with E_{sum} values higher than 10 eV are also included. No significant matrix effects were observed for carbon concentrations lower than 5 g L^{-1}. When increasing the carbon concentration up to 30 g L^{-1}, the intensity of Se and As lines was futher enhanced up to 16% and 10%, respectively, whereas the intensity of atomic lines with E_{sum} values below 6 eV was depressed up to 15%. Carbon concentrations above 30 g L^{-1} did not produce any further enhancement in matrix effects. In general terms the average emission intensity of ionic lines is almost unaffected by the presence of carbon. Similar behaviour was obtained for citric acid solutions.

Finally, it is interesting to note that when the carbon matrix was introduced into the plasma, stable analyte emission signals were obtained after just one minute. Fast response was also obtained after changing back from the carbon solution to the pure aqueous solution. These findings are quite different from those reported by Larsen et al. [26] and Gammergaard et al. [32], who observed that when changing from a methanol solution to an aqueous solution, stationary As and Se signals were only obtained after 35 minutes of flushing with the aqueous solution. This memory effect was attributed to solvent residues in the sample introduction system and tubing material. In our case, the time required to obtain a stationary signal corresponds with the typical wash-out time of the sample introduction system.

3.2. Origin of the carbon-related matrix effects

In order to explain the results presented in the previous paragraph, both spectral and non-spectral interferences must be considered. To evaluate the spectral interferences, the Se I line at 196.026 nm has been selected. It has been described that this line is interfered by the CO molecular band at 206.760 nm [30]. To evaluate this interference carbon solution (prepared from glycerol) was nebulized and the blank signals for different As and Se wavelengths were measured. Results indicate that the contribution of the CO molecular band on the emission signal at 196.026 nm was practically negligible (≈1%). Similar results were obtained using solutions with higher carbon content. No significant spectral interferences were found for the Se and As lines reported in Table 2.

Non-spectral matrix effects are related to changes in the aerosol characteristics and transport to the plasma and/or on the plasma excitation conditions. Therefore, in order to evaluate these effects, experiments were performed to characterize both the primary and tertiary aerosol drop size distributions and to determine the solvent and analyte transport rate (S_{tot} and W_{tot}, respectively) [33].

Fig. 3 shows the DSD curves for the primary (pDSD) and tertiary (tDSD) aerosols obtained with pure aqueous and 20 g L^{-1} carbon containing solutions. Results in this figure indicate that the presence of glycerol does not modify the pDSD. To explain these results, it must be taken into account that, for given experimental conditions, the characteristics of the pneumatically generated aerosols depend on the physical properties of the solution, mainly the surface tension [34]. Aqueous solution and glycerol solution containing 20 g L^{-1} carbon show similar surface tension values (i.e. 72 dynes cm^{-1}) and therefore no difference in the pDSD is expected [35]. Once the primary aerosol is generated, its characteristics are modified along the aerosol pathway to the plasma due to the influence of transport phenomena [36]. For a given pDSD, the significance of these phenomena mainly depends on the solution volatility and density. High volatility allows more solvent evaporation and reduces the droplet surface and therefore also the aerosol size, whereas high solution density can enhance the aerosol losses along the sample introduction

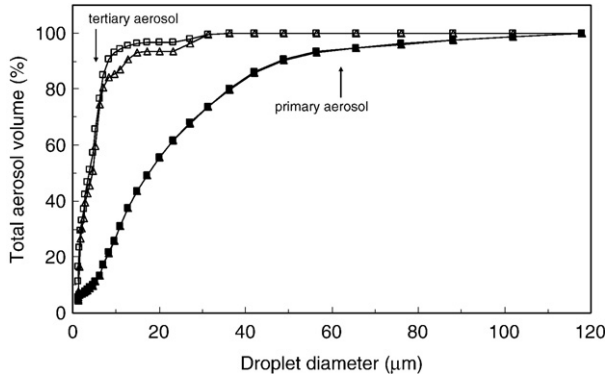

Fig. 3. Volume drop size distribution of the aerosols obtained from an aqueous ((■) primary; (□) tertiary) and a carbon 20 g L^{-1} ((▲) primary; (△) tertiary) solutions. Carbon source: glycerol; Q_g 0.7 L min^{-1}; Q_l 1.0 mL min^{-1}.

system. These physical properties are also similar for the pure aqueous and the carbon solutions (differences in density were not more than 2% whereas the presence of glycerol did not significantly modify the solution volatility since its boiling point is 290 °C). As a consequence, differences in tDSD are not observed (Fig. 3). Based on the comments made above, similar solution transport rate values are expected for both the aqueous and carbon solutions tested. Measured S_{tot} and W_{tot} values are in agreement with this prediction. Thus, operating at a sample uptake rate (Q_l) of 1.0 mL min^{-1} S_{tot} was 24.5±0.6 and 25.3±0.6 mg min^{-1} for the aqueous and the carbon containing solution, respectively. Regarding the analyte transport rate, operating at Q_l of 1.0 mL min^{-1} and using both Mn and Cu as test elements, W_{tot} values were 1.25±0.05 and 1.30±0.05 mg min^{-1}, for the aqueous and the carbon solutions, respectively. From these results it can be concluded that the different I_{rel} values obtained for the atomic lines must be related to plasma phenomena.

Some authors have pointed out that when working with organic compounds, the dissociation of the solvent molecules can increase the plasma thermal conductivity and, as a consequence, plasma peripheral regions may cool down, causing the plasma volume to shrink. This process eventually results in a more compact hotter plasma (thermal pinch effect) [37]. Nevertheless, a careful visual plasma inspection indicates that there is no change in the plasma physical characteristics when changing from pure aqueous to carbon containing solutions.

In order to obtain more information about the plasma characteristics, the Mg II (280.271 nm)/Mg I (285.213 nm) line intensity ratio and the intensity of the Ar I line at 420.069 nm have been measured [38,39]. When increasing the carbon concentration, the argon emission intensity was decreased, thus indicating a reduction in plasma energetic conditions [11,39]. For instance, the Ar emission intensity for the carbon 20 g L^{-1} solution was 10% lower than for the pure aqueous one. These findings are as expected, taking into account that when a concomitant element is introduced in the plasma discharge zone, the plasma temperature, as well as, the atomization/ionization/excitation conditions can be altered. The energy required for the decomposition of glycerol molecules in the plasma is higher than for water. Dissociation energy for the carbon–carbon bond and carbon–hydrogen bond are 6.4 and 3.5 eV, respectively, whereas the energy required to dissociate the oxygen–hydrogen bound is 4.5 eV. Therefore, it would be reasonable to expect higher matrix effects on the emission intensity of ionic lines since they are more sensitive to plasma energetic conditions. In addition, it is difficult to explain why atomic lines of different E_{sum} values behave differently. Plasma status can be also monitored measuring the Mg II/Mg I line intensity ratio. The higher the ratio, the higher the energetic plasma capabilities obtained. Therefore, according to the results shown for Ar I emission, lower Mg II/Mg I line intensity ratios are expected for carbon containing solutions than for water. Nevertheless, the results obtained indicate the opposite behavior, being this ratio for the pure aqueous and the carbon containing solution 8.1 and 9.7, respectively. Similar results were obtained using other line intensity ratios (CrII/CrI, ZnII/ZnI, etc.) [40]. To clarify these contradictory results, plasma excitation temperatures should be measured [41]. Unfortunately, the instrument employed did not allow the study of this parameter since the Fe and Sc lines usually employed for this purpose are not available on the CCD detector used by the instrument. Machat et al. [30] and Long et al. [28] reported that the introduction of carbon into the plasma does not affect plasma excitation temperature and electronic density.

Table 3
I_{rel} values and energy levels of the Se and As lines tested

Element/wavelength (nm)	Energy (eV)		I_{rel}
	Lower level	Upper level	
Se 196.026	0.00	6.32	1.23±0.03
Se 203.985	0.25	6.32	1.20±0.02
As 188.979	0.00	6.56	1.12±0.02
As 193.696	0.00	6.40	1.07±0.03
As 191.197	0.00	6.28	1.06±0.02

Carbon matrix: 20 g L^{-1} prepared from citric acid. R.f. power 1450 W; Q_g 0.7 L min^{-1}; Q_l 1.0 mL min^{-1}.

From the results discussed so far it can be concluded that carbon-related matrix effects in ICP-AES do not arise from any spectral interference or non-spectral interference related to the aerosol generation and transport processes. In addition, the interference is not related to changes in plasma energetic conditions. Therefore it seems to be clear that the origin of the matrix effects must be related to changes in the line excitation mechanism. For atomic lines with E_{sum} lower than 6 eV, the emission signal decrease due to the carbon matrix is attributed to a decrease in the population of excited state atoms [28]. Three different possibilities can be considered: (i) ion formation. This hypothesis can be ruled out since emission signals from ionic lines are not affected by the presence of carbon; (ii) formation of stable carbide compounds [28]; and/or (iii) deactivation of excited state atoms by collisions with elemental carbon or carbon radicals [28].

For As and Se lines, there are two different mechanism to explain the emission signal enhancements, i.e., to explain the increase in the excited atoms population. Firstly, energy transfer from C metastable atoms to Se/As atoms could be considered [30]. According to this mechanism, signal from atomic lines with excitation energies close to that of metastable C (i.e., 6.22 eV) will be enhanced. Taking into account the transition energy levels involved at the different wavelengths tested for As (Table 3), the highest signal enhancement factor should be expected for As I 191.197 nm (E_{exc}=6.28 eV) followed by As I 193.696 nm (E_{exc}=6.40 eV) and As I 188.979 nm (E_{exc}=6.56 eV). Nevertheless, results in Table 3 indicate that the highest signal enhancement factor for this element (i.e., 12%) is observed for the line with the highest excitation energy (i.e., 188.979 nm). Therefore it can be concluded that the energy transfer mechanism considered is not responsible for these interferences. These findings are in agreement with those previously reported [30]. Machat et al. proposed a second hypothesis based in a two-steps mechanism that simultaneously explain the As and Se signal enhancements observed in both ICP-AES and ICP-MS [30]. In the first step, As and Se, due to their ionization energies close to that of carbon (i.e., 11.26 eV), would suffer from a charge transfer

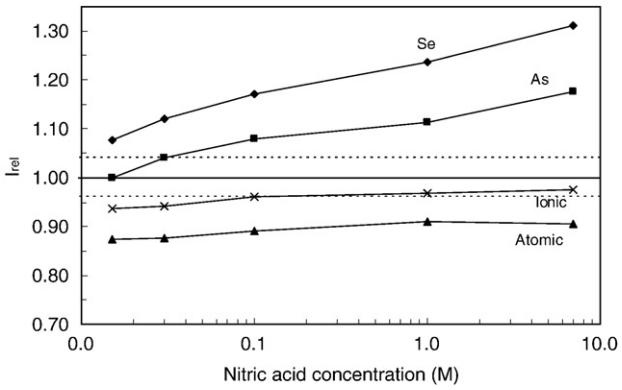

Fig. 4. I_{rel} values as a function of nitric acid concentration for different type of lines using a carbon 20 g L^{-1} solution: (◆) Se I (196.026 nm); (■) As I (188.979 nm); (▲) atomic lines E_{sum}<6 eV; (×) ionic lines. I_{rel} values among dotted lines indicate no matrix effects. Carbon source: glycerol; r.f. power 1450 *W*; Q_g 0.7 L min^{-1}; Q_l 1.0 mL min^{-1}.

reaction from C ions, thus increasing the As^+ and Se^+ populations. It would explain the enhancement in the ion signals observed for these elements in ICP-MS [15,16,18,20,21]. In a second step, these ions would suffer from subsequent ion/electron recombinations thus increasing the population of the excited atoms. This mechanism suggests that the highest signal enhancement factors would be observed for the wavelengths involving the highest upper level energies, irrespective of its lower level energy [30]. This hypothesis is confirmed by the results shown in Table 3. Indeed, Table 3 shows that for As, the signal enhancement factors follow the order: As 188.979 nm > As 193.696 > As 191.197 nm, according to their respective upper level energy values. For Se at the two wavelengths tested, the signal enhancement factor are similar (i.e., about 20%) in spite of their different lower level energy (0.00 and 0.25 eV for Se 196.026 and Se 203.985, respectively).

3.3. Influence of the carbon source

Fig. 1 shows that the magnitude of the matrix effects for As and Se lines depends on the carbon source employed (glycerol and citric acid). Thus, signal enhancements for Se and As atomic lines were more significant for the citric acid solution than for glycerol. For the remaining lines tested (both atomic and ionic), no significant effect of the carbon source on I_{rel} is observed. To explain these results, it must be firstly considered that both matrix solutions show similar physical properties (i.e., surface tension and viscosity) in the carbon concentration range studied and, consequently, no differences in the aerosol characteristics are observed. Nevertheless, the acidity of the citric acid solution was higher than the acidity of the glycerol solution (the pH of these solutions were 1.3 and 2, respectively). To evaluate the influence of the solution pH on carbon based matrix effects, a glycerol solution containing 20 g L^{-1} of carbon was prepared with different concentrations of nitric acid. Fig. 4 shows the influence of the nitric acid concentration on the I_{rel} values for the different groups of lines tested. In this figure it can be observed that atomic lines with E_{sum} below 6 eV and ionic lines were not significantly influenced by the solution pH. However, for As and Se lines, higher I_{rel} values were obtained when the acid concentration was increased. Thus, for instance for Se 196.026 nm, I_{rel} values for a nitric acid concentration of 0.015 M and 7 M were 1.08±0.03 and 1.30±0.03, respectively. When comparing the I_{rel} values shown in Fig. 1 for citric acid with those in Fig. 4 using a glycerol solution with a nitric acid concentration of 0.1 M (i.e., with similar pH values) it can be observed that I_{rel} values are indeed similar. Thus, I_{rel} for Se and As lines measured in the presence of citric acid were 1.23±0.03 and 1.08±0.02 respectively (Fig. 1) whereas the corresponding values for the glycerol solution with similar pH were 1.18±0.03 and 1.08±0.02, respectively. To explain these results it should be noted that no influence of the acid concentration on the primary and tertiary aerosol DSD was observed. Nevertheless, there is a clear effect of the solution acidity on S_{tot}. Thus, S_{tot} value, and therefore the amount of carbon reaching the plasma, measured with the glycerol solution in nitric acid 7 M was 10% higher than that with the same solution in 0.015 M nitric acid. This behaviour can be explained in terms of Coulomb droplet fission [42]. Owing to the aerosol generation process, droplets generated pneumatically have a net electrical charge on their surface. This electrical charge is higher for solutions containing protons, thus increasing the Coulomb fission frequency. Hence, a larger number of small droplets will be generated and higher amount of solvent will be transported to the plasma, increasing carbon based matrix effects.

Potassium hydrogen phthalate was also employed as an alternative carbon source. Using a carbon 20 g L^{-1} solution, the intensity of atomic lines was not affected by the presence of carbon, regardless of their E_{sum} value. However, the intensity for ionic lines was depressed by 13%. These differences can be explained by the presence of potassium in the test solutions, since it is well-known that easily ionisable elements (EIEs) are important interferents in ICP-AES [43,44]. In order to evaluate the influence of potassium on the I_{rel} values when using the phthalate matrix, 8 g L^{-1} of K was added to a carbon 20 g L^{-1} solution prepared from glycerol (matching the K concentration in the potassium hydrogen phthalate solution). In the presence of glycerol plus potassium, the I_{rel} values for the different groups of lines were similar to those obtained for the potassium hydrogen phthalate matrix.

These results point out that the differences on carbon matrix effects between the glycerol, citric acid and potassium hydrogen phthalate solutions depend on the presence of concomitant ions (i.e. H^+, K^+) and not on the carbon source itself.

3.4. Influence of the experimental conditions and sample introduction system

Experimental conditions (i.e. r.f. power, nebulizer gas flow and sample uptake rate) and sample introduction system exert an important influence on the amount of sample that reaches the plasma.

Several r.f. plasma powers in the range of 950 and 1450 W were tested but no significant influence of this parameter on the magnitude of carbon matrix effects was observed. The I_{rel} values were similar to those shown in Fig. 1 for each selected r.f.

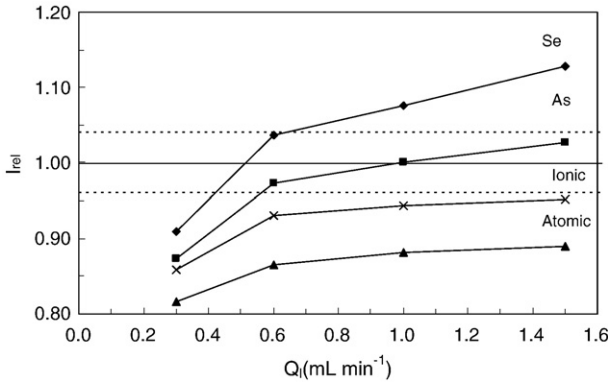

Fig. 5. Influence of Q_l on the I_{rel} values for different type of lines using a carbon 20 g L^{-1} solution: (♦) Se I (196.026 nm); (■) As I (188.979 nm); (▲) atomic lines E_{sum}<6 eV; (×) ionic lines. I_{rel} values among dotted lines indicate no matrix effects. Carbon source: glycerol; solution pH: 2; r.f. power 1450 W; Q_g 0.7 L min^{-1}.

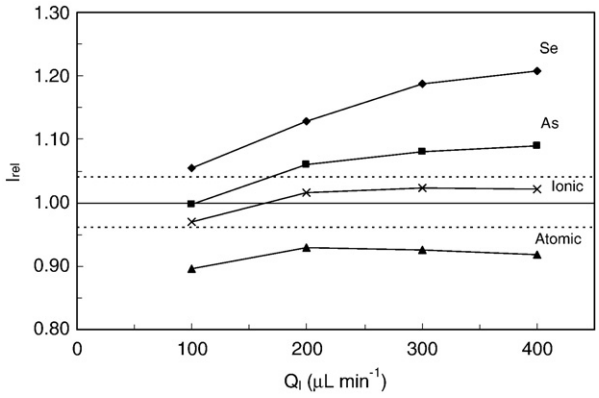

Fig. 6. Influence Q_l on the I_{rel} values for different type of lines with a HEN using a carbon 20 g L^{-1} solution: (♦) Se I (196.026 nm); (■) As I (188.979 nm); (▲) atomic lines E_{sum}<6 eV; (×) ionic lines. I_{rel} values among dotted lines indicate no matrix effects. Instrument: Optima 4300DV. Carbon source: glycerol; solution pH: 2; Q_g 0.6 L min^{-1}. Spray chamber: standard cyclonic (25 °C).

power. These results are in agreement with those previously discussed indicating that carbon solutions do not alter the plasma excitation conditions [30].

Nebulizer gas flow, Q_g, determines the amount of aerosol reaching the plasma. Operating at high Q_g the aerosol drop size distribution becomes finer and the aerosol transport efficiency to the plasma improves. Therefore, when increasing Q_g, higher carbon loading of the plasma and thus, more pronounced matrix effects are expected. However, taking into account signal precision, no influence of this parameter on matrix effects was observed in the Q_g range tested. Thus, for instance, I_{rel} values for atomic lines with E_{sum} values lower than 6 eV operating at Q_g values of 0.7 and 0.5 L min^{-1} were 0.87±0.03 and 0.91±0.03, respectively.

Fig. 5 shows the influence of Q_l on I_{rel} for the different groups of lines tested. As a general trend, results in Fig. 5 indicate that I_{rel} increases with increasing Q_l. At this point, it is important to note that the precision of the I_{rel} values at 0.3 mL min^{-1} was poor (RDS 3.5%) in comparison to the precision at the remaining conditions (2% RSD) since the aerosol generation was not stable. From Fig. 5, it can be observed that for atomic lines with E_{sum}<6 eV as well as for As and ionic lines there is no significant influence of Q_l on the matrix effects. For Se 196.026 nm, I_{rel} was enhanced from 1.04±0.03 to 1.13±0.03 when Q_l was increased from 0.6 up to 1.5 mL min^{-1}. In order to explain these results it should be noted that when Q_l increases, a higher amount of solvent, as well as matrix (i.e. carbon), is loaded into the plasma. At Q_L 1.5 mL·min^{-1} S_{tot} was 15% higher than at 0.6 mL min^{-1}. The emission intensity of carbon at 193.030 nm increases 2.0 times when Q_l is increased from 0.6 mL min^{-1} to 1.5 mL min^{-1}.

In order to evaluate carbon matrix effects under low Q_l conditions, a high efficiency nebulizer (HEN) especially designed for working at uptake rates from 0.1 up to 0.4 mL min^{-1} coupled to a cyclonic spray chamber was used. Fig. 6 shows the influence of Q_l on the I_{rel} values using this arrangement. When comparing the results shown in Figs. 5 and 6, it can be observed that the behaviour is almost the same. Nevertheless, when working with the HEN, carbon matrix effects are higher for Se and As lines, (up to 20% and 10%, respectively, for HEN). To explain these differences, it must be considered that the special design of the HEN gives rise to finer primary aerosols than those generated with the conventional nebulizer operating at low sample uptake rates [45]. As a consequence, the aerosol transport rate to the plasma is improved [46,47]. From these statements, it is understandable that carbon matrix effects are more significant for the HEN than for the pneumatic nebulizer, since a higher amount of carbon is transported to the plasma with this nebulizer.

To evaluate the influence of the spray chamber design on carbon-related matrix effects, a low volume cyclonic spray chamber (i.e. Cinnabar) attached to the HEN was employed. Table 4 shows the I_{rel} values obtained for the different groups of lines tested as a function of the spray chamber temperature with the Cinnabar. When comparing I_{rel} values for Se and As using this spray chamber at ambient temperature to those obtained with the standard cyclonic spray chamber under the same conditions (Fig. 6), it can be concluded that matrix effects are higher for the standard cyclonic than for the cinnabar spray chamber. Thus, at 25 °C and 400 μL min^{-1} the I_{rel} values for Se were 1.21±0.03 and 1.08±0.03, for the standard cyclonic spray chamber and the Cinnabar respectively. Similar behaviour was observed for the As lines. For the remaining atomic and ionic lines, no significant differences were observed between both sample introduction systems. Maestre et al. [48,49] pointed out that spray chamber characteristics play a significant role on the non-spectral matrix

Table 4
I_{rel} values for different emission lines as a function of the spray chamber temperature

Type of line	Temperature (°C)		
	25	35	45
Se I (196.026 nm)	1.08±0.03	1.17±0.03	1.15±0.03
As I (188.979 nm)	1.02±0.03	1.10±0.03	1.09±0.04
Atomic	0.93±0.03	0.95±0.04	0.94±0.04
Ionic	0.98±0.04	1.00±0.03	0.97±0.04

Carbon matrix: 20 g L^{-1} prepared from glycerol. Instrument: Optima 4300DV. Spray chamber: Cinnabar. Solution pH 2. R.f. power 1450 W; Q_g 0.6 L min^{-1}; Q_l 0.4 mL min^{-1}.

effects since its design modifies the aerosol transport along the aerosol pathway towards the plasma. The Cinnabar spray chamber was especially designed to work at low uptake rates and to increase the analysis throughput. For this reason, its inner volume (19 mL) is lower than for the standard cyclonic spray chamber (33 mL). A reduction of the spray chamber volume may enhance aerosol losses against the spray chamber walls, thus decreasing the aerosol transport and, hence, the amount of carbon loading to the plasma [50]. From these results it can be concluded that the Cinnabar spray chamber seems a good choice to reduce carbon-related interferences.

Aerosol transport to the plasma can also be modified by heating or cooling of the spray chamber. Higher temperatures enhance solvent evaporation from the aerosol droplet surface thus improving the aerosol transport to the plasma. Therefore, carbon-related matrix effects are expected to be enhanced by increasing the spray chamber temperature. This hypothesis is confirmed by the results shown in Table 4. Thus, when the spray chamber temperature is increased from 25° to 35 °C the carbon matrix effects are enhanced. Indeed, the emission intensity of the C I 193.030 nm line increases 1.7 times when the spray chamber temperature is increased from 25 °C to 35 °C. Temperatures above 35 °C do not produce any further increase in matrix effects and the plasma also becomes unstable.

3.5. Analysis of a certified Se-enriched yeast

The presence of carbon in the sample is a potential source of error in ICP-AES. To evaluate the influence of carbon-related matrix effects on the results of elemental analysis of biological samples, a Se enriched-yeast certified material was analyzed. Because of the low sensitivity of the Se lines, the experimental conditions were selected to obtain the best limits of detection (i.e. r.f. power 1450 W, Q_g of 0.7 L min^{-1} and a Q_l 1 mL min^{-1}) irrespective of the magnitude of the carbon-related interferences.

Several calibration strategies were evaluated. First of all, the yeast sample was analyzed using pure aqueous and carbon matched standards. In order to prepare the carbon matched standards, the amount of carbon present in the certified sample was determined by measuring the C I 193.030 nm emission line intensity in the digested samples. The carbon content in the sample solution was approximately of 15 g L^{-1}. Thus, standards with this carbon concentration were prepared from glycerol.

Table 5
Results of Se-enriched certified yeast analysis using different calibration strategies and certified analyte concentrations values

Methodology	Concentration (mg L^{-1})	
	Se (196.026 m)	Se (203.985 m)
Certified	2059±64	2059±64
Aqueous standards	2490±80	2400±100
Carbon matched standards [a]	1950±60	1900±100
Carbon buffered standards [b]	1830±140	1840±150

Matrix: nitric acid 7 M and hydrochloric 1.5 M. R.f. power 1450 W; Q_g 0.7 L min^{-1}; Q_l 1.0 mL min^{-1}.
[a] Carbon concentration 15 g L^{-1}.
[b] Carbon concentration 30 g L^{-1}.

Nitric acid and hydrochloric acid mixture (3:1) was employed to digest the yeast sample. As it has been demonstrated (Fig. 4), carbon-related matrix effects depend on the solution pH. Therefore, both the aqueous and the carbon containing standards were prepared with the appropriate acid mixture to match the acid content in the digested samples (i.e. nitric acid 7 M and hydrochloric acid 1.5 M). Also several EIEs were found in the yeast sample (i.e. K, Na, Ca, Mg) but the salt concentration in the digested sample was not high enough (i.e. potassium content lower than 300 mg L^{-1}) to produce any significant additional matrix effect. Table 5 shows the results of the Se determination in the certified yeast when aqueous and carbon 15 g L^{-1} standards are employed, as well as the Se certified value. It can be concluded that calibration with carbon matched standards allowed the accurate determination of Se within a confidence level of 95% (3 replicates). However, when pure aqueous standards were used, the Se concentration found was 20% higher than the certificated value. It is interesting to note that this error is higher than that expected from the results shown in Fig. 2 (i.e. 6% signal enhancement) due to the lower pH of the sample solution analyzed.

Although we have demonstrated that matrix matched standards allow the accurate determination of selenium in the yeast sample, the analysis throughput is considerably reduced using this approach. To overcome this drawback, two additional calibration strategies were considered. In principle, internal standardization can be used [51,52] but, unfortunately, it is not possible to find any atomic line that behaves similar to Se lines. Therefore, another methodology was tested, based on the results shown in Fig. 2, where it can be observed that the presence of carbon in higher concentrations ($\geq$30 g L^{-1}) would cause similar of matrix effects on the Se emission intensity. Adjusting the carbon concentration to values higher than 30 g L^{-1} in both sample and standards would thus allow calibration without the need to consider the initial carbon content of the sample. To evaluate this approach, a glycerol solution was added to the digested yeast samples to achieve a final extra carbon concentration of 30 g L^{-1}. Calibration standards were prepared in a carbon solution of 30 g L^{-1}, also from glycerol, and the appropriate acid mixture to match the acid content to the digested yeast sample. Table 5 shows the results obtained using this calibration strategy (i.e. carbon buffered standards). As it can be observed Se concentration values obtained using this approach were in agreement with those certified for a confidence level of 95% (3 replicates).

4. Conclusions

From the results obtained in the present work it can be concluded that carbon-related matrix effects in ICP-AES depend on: (i) the characteristics of the emission line employed. Emission signals for atomic lines are depressed or enhanced depending on their excitation energies. Thus, the presence of carbon in the matrix gives rise to a decrease in the emission signal of atomic lines with excitation energies lower than 6 eV. For atomic lines with excitation energies above 6 eV (i.e. Se and As), the presence of carbon gives rise to an increase in the

emission signals up to 23%. Ionic lines are almost unaffected by the presence of carbon; (ii) the amount of carbon introduced in the plasma. The higher the carbon concentration, the higher the matrix effect observed. Nevertheless, carbon concentrations above 30 g L^{-1} did not produce any further enhancement in the matrix effects. In addition, matrix effects increase when using high sample uptake rates, as well as, high efficiency nebulizers; and (iii) the concomitant elements present in the carbon matrix (i.e. K^+ or H^+). Thus, matrix effects for atomic lines with E_{sum} values higher than 6 eV were more significant for citric acid than for glycerol since the lower solution acidity of the former increased carbon transport to the plasma. No differences in the aerosol characteristics and in the analyte and solvent transport efficiencies were observed between pure aqueous and carbon containing solutions. In addition, no evidences of plasma energetic characteristics changes have been obtained. Therefore, the origin of the carbon interferences is attributed to changes in the element excitation mechanisms due to the presence of carbon in the matrix. Finally, in order to successfully perform the analysis of carbon-containing samples (biological, petrochemical, etc.), the calibration methodology is the key subject. By addition of a given amount of carbon to both samples and standards the interference effect can be buffered so that the emission signal is independent of the initial carbon content in the sample. Using this approach, accurate Se determination is achieved by using one set of carbon matrix matched standards, irrespective of the carbon concentration of the individual samples.

Acknowledgement

G. Grindlay thanks the University of Alicante for the fellowship.

References

[1] D.G.J. Weir, M.W. Blades, The response of the inductively coupled argon plasma to solvent plasma load: spatially resolved maps of electron density obtained from the intensity of one argon line, Spectrochim. Acta Part B 49 (1994) 1231–1250.
[2] D.G.J. Weir, M.W. Blades, Characteristics of an inductively coupled argon plasma operating with organic aerosol: Part 1. Spectral and spatial observations, J. Anal. At. Spectrom. 9 (1994) 1311–1322.
[3] J. Mora, J.L. Todolí, A. Canals, V. Hernandis, Comparative study of several nebulizers in inductively coupled plasma atomic emission spectrometry: low-pressure versus high-pressure nebulization, J. Anal. At. Spectrom. 12 (1997) 445–451.
[4] G. Grindlay, S. Maestre, L. Gras, J. Mora, Introduction of organic solvent solutions into inductively coupled plasma-atomic emission spectrometry using a microwave assisted sample introduction system, J. Anal. At. Spectrom. 21 (2006) 1403–1411.
[5] A.W. Boorn, M.S. Cresser, R.F. Browner, Evaporation characteristics of organic aerosol used in analytical atomic spectrometry, Spectrochim. Acta Part B 35 (1980) 823–832.
[6] R.I. McCrindle, C.J. Rademeyer, Analytical parameters of ethanol solutions in a 40 MHz inductively coupled plasma optical emission spectrometer, J. Anal. At. Spectrom. 11 (1996) 437–444.
[7] M.W. Blades, B.L. Caughlin, Excitation temperature and electron density in the inductively coupled plasma—aqueous vs organic solvent introduction, Spectrochim. Acta Part B 40 (1985) 579–591.
[8] C. Pan, G. Zhu, R.F. Browner, Role of auxiliary gas flow in organic sample introduction with inductively coupled plasma atomic emission spectrometry, J. Anal. At. Spectrom. 7 (1992) 1231–1237.
[9] J. Mora, I. Rico, A. Canals, Aerosol desolvation studies with a thermospray nebulizer coupled to inductively coupled plasma atomic emission spectrometry, Analyst 123 (1998) 1229–1234.
[10] R.I. Botto, J.J. Zhu, Use of an ultrasonic nebulizer with membrane desolvation for analysis of volatile solvents by inductively coupled plasma atomic emission spectrometry, J. Anal. At. Spectrom. 9 (1994) 905–912.
[11] D.R. Wiederin, R.S. Houk, R.K. Winge, A.P. D'Silva, Introduction of organic solvents into inductively coupled plasmas by ultrasonic nebulization with cryogenic desolvation, Anal. Chem. 62 (1990) 1155–1160.
[12] E. Evans, L. Ebdon, Effect of organic solvents and molecular gases on polyatomic ion interferences in inductively coupled plasma mass spectrometry, J. Anal. At. Spectrom. 5 (1990) 425–430.
[13] V.L. Dressler, D. Pozebon, A.J. Curtius, Introduction of alcohols in inductively coupled plasma mass spectrometry by a flow injection system, Anal. Chim Acta 379 (1999) 175–183.
[14] S.D. Olsen, S. Westerlund, R.G. Visser, Analysis of metals in condensates and naphta by inductively coupled plasma mass spectrometry, Analyst 122 (1997) 1229–1234.
[15] Z. Hu, S.H.S. Gai, Y. Liu, S. Lin, Volatile organic solvent-induced signal enhancements in inductively coupled plasma-mass spectrometry: a case study of methanol and acetone, Spectrochim. Acta Part B 59 (2004) 1463–1470.
[16] P. Allain, L. Jaunault, Y. Mauras, J.M. Mermet, T. Delaporte, Signal enhancement of elements due to the presence of carbon-containing compounds in inductively coupled plasma mass spectrometry, Anal. Chem. 63 (1991) 1497–1498.
[17] B. Gammelgard, O. Jons, Determination of selenium in urine by inductively coupled plasma mass spectrometry: interferences and optimization, J. Anal. At. Spectrom. 14 (1999) 867–874.
[18] M. Kovacevic, W. Goessler, N. Mikac, M. Veber, Matrix effects during phosphorus determination with quadrupole inductively coupled plasma mass spectrometry, Anal. BioAnal. Chem. 383 (2005) 145–151.
[19] M. Pettine, B. Casentini, D. Mastroianni, S. Capri, Dissolved inorganic carbon effect in the determination of arsenic and chromium in mineral waters by inductively coupled plasma-mass spectrometry, Anal. Chim. Acta 599 (2007) 191–198.
[20] F.R. Abou-Shakra, M.P. Rayman, N.L. Ward, V. Hotton, G. Bastian, Enzymatic digestion for the determination of trace elements in blood serum by inductively coupled plasma mass spectrometry, J. Anal. At. Spectrom. 9 (1997) 429–433.
[21] A.S. Al-Ammar, E. Reitznerova, R.M. Barnes, Feasibility of using beryllium as internal reference to reduce non-spectroscopic carbon species matrix effects in the inductively coupled plasma-mass spectrometry (ICP-MS) determination of boron in biological samples, Spectrochim. Acta Part B 54 (1999) 1813–1820.
[22] I. Llorente, M. Gómez, C. Cámara, Improvement of selenium determination in water in inductively coupled plasma mass spectrometry through use of organic compounds as matrix modifiers, Spectrochim. Acta Part B 52 (1997) 1825–1838.
[23] B. Gammelgaard, O. Jons, Comparison of an ultrasonic nebulizer with a cross-flow nebulizer for selenium speciation by ion-chromatography and inductively coupled plasma mass spectrometry, J. Anal. At. Spectrom. 15 (2000) 499–505.
[24] M. Kovacevic, W. Goessler, Direct introduction of volatile carbon compounds into the spray chamber of an inductively coupled plasma mass spectrometer: sensitivity enhancement for selenium, Spectrochim. Acta Part B 60 (2005) 1357–1362.
[25] S. Cao, H. Chen, X. Zeng, Determination of mercury in biological samples using organic compounds as matrix modifiers by inductively coupled plasma mass spectrometry, J. Anal. At. Spectrom. 14 (1999) 1183–1186.
[26] E.H. Larsen, S. Stürup, Carbon-enhanced inductively coupled plasma mass spectrometric detection of arsenic and selenium and its application to arsenic speciation, J. Anal. At. Spectrom. 9 (1994) 1099–1105.
[27] E. Warbuton, H. Goenaga-infante, Methane mixed plasma — improved sensitivity of inductively coupled plasma mass spectrometry detection for selenium speciation analysis of wheat-based food, J. Anal. At. Spectrom. 22 (2007) 370–376.
[28] G.L. Long, J.S. Bolton, The effect of propane on atomic spectrometric signals in the inductively coupled argon plasma, Spectrochim. Acta Part B 42 (1987) 581–589.

[29] J. Machat, V. Kanicky, V. Otruba, Determination of selenium in blood serum by inductively coupled plasma atomic emission spectrometry with pneumatic nebulization, Anal. Bioanal. Chem 372 (2002) 576–581.
[30] J. Machat, V. Otruba, V. Kanicky, Spectral and non-spectral interferences in the determination of selenium by inductively coupled plasma atomic emission spectrometry, J. Anal. At. Spectrom. 17 (2002) 1096–1102.
[31] R.F. Browner, Fundamental aspects of aerosol generation and transport, in: P.W.J.M. Boumans (Ed.), Inductively Coupled Plasma Emission Spectrometry. Part II: Applications and Fundamentals, Chapter 8, Wiley, 1987, p. 244.
[32] B. Gammelgaard, O. Jons, Determination of selenium in urine by inductively coupled plasma mass spectrometry: interferences and optimization, J. Anal. At. Spectrom. 14 (1999) 867–874.
[33] J. Mora, S. Maestre, V. Hernandis, J.L. Todolí, Liquid-sample introduction in ICP-AES, Trends in Anal. Chem. 22 (2003) 123–132.
[34] J. Mora, V. Hernandis, A. Canals, Influence of solvent physical properties on drop size distribution, transport and sensitivity in flame atomic absorption spectrometry with pneumatic nebulisation, J. Anal. At. Spectrom. 6 (1991) 573–579.
[35] B. Sharp, Pneumatic nebulisers and spray chambers for inductively coupled plasma spectrometry. A review. Part 1. Nebulisers, J. Anal. At. Spectrom. 3 (1988) 613–652.
[36] R.F. Browner, A.W. Boorn, D.D. Smith, Aerosol transport model for atomic spectrometry, Anal. Chem. 54 (1982) 1411–1419.
[37] S. Greenfield, H.M. McGeachin, Calorimetric and dimensional studies on inductively coupled plasmas, Anal. Chim. Acta 100 (1978) 101–119.
[38] J.M. Mermet, Use of magnesium as a test element for inductively coupled plasma atomic emission spectrometry diagnostics, Anal. Chim. Acta 250 (1991) 85–94.
[39] A. Batal, J. Jarosz, J.M. Mermet, A spectrometric study of a 40 MHz inductively coupled plasma—VI. Argon continuum in the visible region of the spectrum, Spectrochim. Acta Part B 36 (1981) 983–992.
[40] E.H. van Veen, M.T.C. de Loos-Vollebregt, On the use of line intensity ratios and power adjustments to control matrix effects in inductively coupled plasma optical emission spectrometry, J. Anal. At. Spectrom. 14 (1999) 831.
[41] J.M. Mermet, in: S. Hill (Ed.), Inductively Coupled Plasma Spectrometry and Its Applications, Blackwell publishing, Oxford, 2007, p. 27, Chapter 2.
[42] Q. Xu, D. Balik, G.R. Agnes, Aerosol static electrification and its effects in inductively coupled plasma spectroscopy, J. Anal. At. Spectrom. 16 (2001) 715–723.
[43] K.P. Li, J.D. Hwang, J.D. Winefordner, Studies of chemical interferences in an inductively coupled plasma using moment analysis of space-resolved emission profiles, Anal. Chem. 62 (1990) 1233–1238.
[44] J.L. Todolí, L. Gras, V. Hernandis, J. Mora, Elemental matrix effects in ICP-AES, J. Anal. At. Spectrom. 17 (2002) 142–169.
[45] J.L. Todolí, J.M. Mermet, Sample introduction systems for the analysis of liquid microsamples by ICP-AES and ICP-MS, Spectrochim. Acta Part B 61 (2006) 239–283.
[46] H. Liu, A. Montaser, Phase-doppler diagnostic studies of primary and tertiary aerosols produced by a high-efficiency nebulizer, Anal. Chem. 66 (1994) 3233–3242.
[47] J.W. Olesik, J.A. Kinzer, B. Harkleroad, Inductively coupled plasma optical emission spectrometry using nebulizers with widely different sample consumption rates, Anal. Chem. 66 (1994) 2022–2030.
[48] S. Maestre, J. Mora, L. Gras, J.L. Todolí, Study of matrix effects produced by inorganic species in inductively coupled plasma atomic emission spectrometry with several spray chambers, Can. J. Anal. Sci. Spectrosc. 45 (2000) 124–132.
[49] S. Maestre, J. Mora, J.L. Todolí, Studies about the origin of the non-spectroscopic interferences caused by sodium and calcium in inductively coupled plasma atomic emission spectrometry. Influence of the spray chamber design, Spectrochim. Acta Part B 57 (2002) 1753–1770.
[50] J.L. Todolí, S. Maestre, J. Mora, A. Canals, V. Hernandis, Comparison of several spray chambers operating at very low liquid flow rates in inductively coupled plasma atomic emission spectrometry, Fresenius, J. Anal. Chem. 368 (2000) 773–779.
[51] M. Grotti, E. Magi, R. Leardi, Selection of internal standards in inductively coupled plasma atomic emission spectrometry by principal component analysis, J. Anal. At. Spectrom. 18 (2003) 274–281.
[52] M. Grotti, R. Frache, Reduction of acid effects in inductively coupled plasma optical emission spectrometry using internal standards selected by principal component analysis, J. Anal. At. Spectrom. 18 (2003) 1192–1197.